Neutrinoless $\beta\beta$ nuclear matrix elements using isovector spin-dipole $J^\pi = 2^-$ data

L. Jokiniemi,[1] H. Ejiri,[2,3] D. Frekers,[4] and J. Suhonen[1]
[1]*Department of Physics, University of Jyväskylä, P.O. Box 35 (YFL), FI-40014 Jyväskylä, Finland*
[2]*Research Center for Nuclear Physics, Osaka University, Ibaraki, Osaka 567-0047, Japan*
[3]*Nuclear Physics, Czech Technical University, Prague, Czech Republic*
[4]*Institut für Kernphysik, Westfälische Wilhelms-Universität, D-48149 Münster, Germany*

(Received 12 April 2018; revised manuscript received 26 June 2018; published 9 August 2018)

Ground-state-to-ground-state neutrinoless double-beta ($0\nu\beta\beta$) decays in nuclei of current experimental interest are revisited. In order to improve the reliability of the nuclear matrix element (NME) calculations for the light Majorana-neutrino mode, the NMEs are calculated by exploiting the newly available data on isovector spin-dipole (IVSD) $J^\pi = 2^-$ giant resonances. In order to correctly describe the IVSD up to and beyond the giant-resonance region, the present computations are performed in extended no-core single-particle model spaces using the spherical version of the proton-neutron quasiparticle random-phase approximation (pnQRPA) with two-nucleon interactions based on the Bonn one-boson-exchange G matrix. The appropriate short-range correlations, nucleon form factors, higher-order nucleonic weak currents, and partial restoration of the isospin symmetry are included in the calculations. The results are compared with earlier calculations of Hyvärinen and Suhonen [Phys. Rev. C **91**, 024613 (2015)] performed in much smaller single-particle bases without access to the IVSD $J^\pi = 2^-$ giant-resonance data reported here.

DOI: 10.1103/PhysRevC.98.024608

I. INTRODUCTION

The neutrinoless double-beta ($0\nu\beta\beta$) decay of atomic nuclei is a promising way to access the physics beyond the standard model [1–5], as witnessed by the ever growing experimental interest in this decay mode. At the same time half-lives of the two-neutrino $\beta\beta$ ($2\nu\beta\beta$) decays of several nuclei have been measured with increased precision [6,7]. Important nuclei for the present $0\nu\beta\beta$ experiments are ^{76}Ge, ^{82}Se, ^{96}Zr, ^{100}Mo, ^{116}Cd, ^{130}Te, and ^{136}Xe [8].

There are many models which have recently been used to compute the $0\nu\beta\beta$ nuclear matrix elements (NMEs): the quasiparticle random-phase approximation (QRPA), as well as its proton-neutron version (pnQRPA) (see, e.g., [9]) and its renormalized extensions [10,11], the interacting shell model (ISM) [12,13], the microscopic interacting boson model (IBA-2) [14], the Gogny-based energy-density functional (EDF) [15] and its variation [16], and the projected Hartree-Fock-Bogoliubov mean-field scheme (PHFB) [17]. Very recently also the beyond-mean-field covariant density functional theory [18,19] and advanced shell-model frameworks [20–23] have been used to describe the $0\nu\beta\beta$ NMEs of nuclei. For more details see the reviews [5,24].

The pnQRPA has several advantages in calculating the $2\nu\beta\beta$ and $0\nu\beta\beta$ NMEs:

(i) In the pnQRPA calculations one avoids the use of the closure approximation,
(ii) pnQRPA can accommodate large single-particle bases, including all the relevant spin-orbit-partner orbitals [25,26], and
(iii) the gross features of the distribution of nuclear states can be reliably accounted for by the pnQRPA [27] although the model may fail to predict properties of individual states.

The features (i)–(iii) of the pnQRPA make it an ideal nuclear model to combine the $2\nu\beta\beta$ and $0\nu\beta\beta$ calculations in a consistent way. The relation of the pnQRPA Hamiltonian and the $2\nu\beta\beta$ decay was further deepened in the work of Ref. [28] where a partial isospin-restoration scheme for the pnQRPA was proposed. This same method was later used by Hyvärinen *et al.* [29] for pnQRPA-based and in Barea *et al.* [30] for IBM-2 based $0\nu\beta\beta$-decay calculations.

A key parameter of the pnQRPA is the particle-hole parameter $g_{\rm ph}$ associated with the spin-isospin correlations and the location [31] of the giant resonances. So far in the calculations the value of this parameter has been fixed by fitting the location of the Gamow-Teller giant resonance (GTR). The fitted value, $g_{\rm ph}(1^+)$, together with the value of the particle-particle parameter $g_{\rm pp}$ of the pnQRPA, fixes the contribution of the 1^+ channel to the $0\nu\beta\beta$ NME. However, the 1^+ contributions to the $0\nu\beta\beta$ NME are in many cases (much) smaller than the contributions from the 2^- isovector spin-dipole (IVSD) states which play an important role in this NME, in particular for the medium-heavy nuclei (see Fig. 7). Recently data on the location of the IVSD giant resonances became available from charge-exchange reactions performed at the Research Center for Nuclear Physics (RCNP), Osaka, Japan. Here we report for the first time on the values of the $0\nu\beta\beta$ NMEs based on $g_{\rm ph}$ values $g_{\rm ph}(2^-)$, fixed by the observed location of the IVSD giant resonances.

In the present work we compute the $0\nu\beta\beta$ NMEs using the spherical version of pnQRPA framework and the partial isospin-restoration scheme of Ref. [28]. The value of $g_{\rm ph}$

is determined by the empirical locations of the $J^\pi = 1^+$ GTR and the $J^\pi = 2^-$ IVSD giant resonance. The isoscalar part of the particle-particle parameter, $g_{\rm pp}^{T=0}$, is fitted to the values of the $2\nu\beta\beta$ matrix elements. The value of the isovector part of the particle-particle parameter, $g_{\rm pp}^{T=1}$, on the other hand, is determined by the isospin-restoration scheme. We extend the studies of [29,32–34] by using large no-core single-particle bases in order to reliably describe the IVSD $J^\pi = 2^-$ giant-resonance region and to see how the extension of the valence space affects the magnitudes of the $0\nu\beta\beta$ NMEs for the nuclei of interest. We also extend our previous work [35] by studying the impact of the value of the parameter $g_{\rm ph}(2^-)$ on the magnitude of the $0\nu\beta\beta$ NME, when adjusted to describe the energy of the measured IVSD $J^\pi = 2^-$ giant resonance separately. All this is done to test the reliability of the $0\nu\beta\beta$ NMEs computed in Ref. [29] and to produce an improved set of NMEs for further use in, e.g., analyses related to the experimental $0\nu\beta\beta$ data.

This article is organized as follows: In Sec. II we briefly introduce the underlying formalism of the $2\nu\beta\beta$ and $0\nu\beta\beta$ decays as well as the IVSD $J^\pi = 2^-$ strength. In Sec. III we discuss the determination of the model parameters, and display and discuss the obtained results for the $0\nu\beta\beta$ NMEs calculated using different single-particle bases and model parameters. The final conclusions are drawn in Sec. IV.

II. COMPUTATIONAL SCHEME

In this section we introduce a brief theoretical outline of our computational scheme. Both the IVSD $J^\pi = 2^-$ and $0\nu\beta\beta$ calculations are based on the spherical version of pnQRPA theory, which is reviewed briefly in the first subsection. In the following subsections we introduce the theoretical aspects of the IVSD $J^\pi = 2^-$ strength, two-neutrino double-beta decay, and neutrinoless double-beta decay, correspondingly.

A. pnQRPA and the Hamiltonian parameters

In this section we explain the spherical version of the pnQRPA procedure briefly, starting from the single-particle bases for protons and neutrons: The single-particle energies for both protons and neutrons, for each even-even nucleus involved, are obtained by solving the radial Schrödinger equation for a Coulomb-corrected Woods-Saxon (WS) potential optimized for nuclei close to the β stability line [36]. This choice is justified since the $\beta\beta$-decaying nuclei lie always rather close to the bottom of the valley of beta stability. We adopt the single-particle bases used in the isovector spin-multipole calculations of [35], i.e., no-core bases with all the orbits from the $N = 0$ oscillator major shell up to at least two oscillator major shells above the respective Fermi surfaces for protons and neutrons. We include in our calculations both the bound and quasibound single-particle states. The same orbitals are used for both neutrons and protons. We perform our calculations, whenever possible, in both the bare Woods-Saxon bases, abbreviated as "WS", and in the slightly modified bases that we used in [35], where the proton/neutron single-particle energies of the orbitals close to the Fermi surfaces were adjusted to better reproduce the low-lying spectra of the neighboring odd-mass nuclei. These bases are abbreviated as "sp" (see Table I). In the cases of mass numbers $A = 96, 100$ the use of the bare Woods-Saxon bases results in a nonphysical $g_{\rm pp}$ behavior of the $2\nu\beta\beta$ results, and we use therefore only the sp bases. On the other hand, for $A = 116$ the use of the bare Woods-Saxon bases results in a good correspondence between the calculated and experimental spectra, so no modifications in the single-particle energies were necessary.

TABLE I. Pairing scaling factors and the resulting pairing gaps for the nuclei relevant for this work. "WS" denotes the Woods-Saxon and "sp" the modified basis.

Nucleus	Basis	$g_{\rm pair}^{(n)}$	$g_{\rm pair}^{(p)}$	Δ_n (MeV)	Δ_p (MeV)
^{76}Ge	WS	1.05	0.89	1.57	1.52
	sp	0.97	0.89		
^{76}Se	WS	1.06	0.91	1.72	1.71
	sp	1.01	0.91		
^{96}Zr	sp	0.73	0.86	0.92	1.48
^{96}Mo	sp	0.90	0.91	1.03	1.52
^{100}Mo	WS	0.85	0.95	1.31	1.63
	sp	0.88	0.96		
^{100}Ru	WS	0.89	0.96	1.27	1.60
	sp	0.85	0.93		
^{116}Cd	WS	0.89	0.93	1.37	1.43
^{116}Sn	WS	0.82	0.89	1.16	1.84
^{128}Te	WS	0.96	0.81	1.30	1.09
	sp	0.86	0.81		
^{128}Xe	WS	0.94	0.88	1.27	1.30
	sp	0.86	0.88		
^{130}Te	WS	0.94	0.78	1.21	1.02
	sp	0.86	0.78		
^{130}Xe	WS	0.95	0.86	1.25	1.26
	sp	0.85	0.86		
^{136}Xe	WS	0.85	0.76	1.44	0.98
	sp	0.84	0.76		
^{136}Ba	WS	0.90	0.83	1.08	1.22
	sp	0.87	0.83		

The quasiparticle spectra for protons and neutrons, needed in the pnQRPA diagonalization, are obtained by solving the BCS equations for protons and neutrons, separately. In our calculations the two-body interaction is derived from the Bonn-A one-boson-exchange potential introduced in [37]. The calculated BCS pairing gaps are fitted (see [31,38–40]) to the phenomenological ones, $\Delta_{\rm n}$ for neutrons and $\Delta_{\rm p}$ for protons, by using adjustable pairing strengths, $g_{\rm pair}^{(n)}$ for neutrons and $g_{\rm pair}^{(p)}$ for protons, in a way described in detail in Ref. [35]. The needed separation energies were taken from [41]. The values of the resulting pairing scaling factors are presented in Table I.

The wave functions and excitation energies for the complete set of J^π excitations in an odd-odd nucleus are obtained by performing a pnQRPA diagonalization in the basis of unperturbed quasiproton-quasineutron pairs coupled to J^π. The spherical pnQRPA states in odd-odd nuclei are then of

the form

$$\left|J_k^\pi M\right\rangle = \sum_{pn}\left[X_{pn}^{J_k^\pi} A_{pn}^\dagger(JM) - Y_{pn}^{J_k^\pi}\tilde{A}_{pn}(JM)\right]|\text{pnQRPA}\rangle, \tag{1}$$

where k numbers the states of the same spin-parity J^π, the amplitudes X and Y are the forward- and backward-going amplitudes, $A^\dagger$ and $\tilde{A}$ the quasiproton-quasineutron creation and annihilation operators, and $|\text{pnQRPA}\rangle$ is the pnQRPA vacuum. M denotes the z projection of J. The formalism is explained in detail in Refs. [31,38].

The X and Y amplitudes in Eq. (1) are calculated by diagonalizing the pnQRPA matrix separately for each multipole J^π. The isoscalar ($T = 0$) and isovector ($T = 1$) parts of the particle-particle G-matrix elements are multiplied by common factors $g_{\text{pp}}^{T=0}$ and $g_{\text{pp}}^{T=1}$, respectively, for all the multipoles. In addition, the particle-hole part was scaled by a common factor g_{ph} for each multipole. These renormalization factors are listed in the following section for each mass number A separately.

B. Isovector spin-dipole $J^\pi = 2^-$ strength

The transition operator for the IVSD ($L = 1$) $J^\pi = 2^-$ transitions is of the form

$$\mathcal{O}_{1,2}^\pm = ir[\boldsymbol{Y}_1\boldsymbol{\sigma}]_2 t_\pm, \tag{2}$$

where $\boldsymbol{Y}_1$ is the spherical harmonic of rank 1, $\boldsymbol{\sigma}$ the Pauli spin operator, r the radial coordinate, and t_+ and t_- are the isospin raising and lowering operators. The reduced single-particle NMEs of this operator are of the form [31,36]

$$\begin{aligned}(j_f\|\mathcal{O}_{1,2}^\pm\|j_i) &= \left(n_f l_f \frac{1}{2} j_f \middle\| ir[\boldsymbol{Y}_1\boldsymbol{\sigma}]_2 \middle\| n_i l_i \frac{1}{2} j_i\right)\\ &= \sqrt{6}\hat{j}_f\sqrt{5}\hat{j}_i\frac{(-1)^{l_f}}{\sqrt{4\pi}}\hat{l}_f\sqrt{3}\hat{l}_i\begin{pmatrix} l_f & 1 & l_i\\ 0 & 0 & 0\end{pmatrix}\\ &\times\begin{Bmatrix} l_f & \frac{1}{2} & j_f\\ l_i & \frac{1}{2} & j_i\\ 1 & 1 & 2\end{Bmatrix}\mathcal{R}_{fi}^{(1)}(-1)^{\frac{1}{2}(l_i-l_f+1)},\end{aligned} \tag{3}$$

where $\hat{j} = \sqrt{2j+1}$, $\mathcal{R}_{fi}^{(1)}$ is a radial integral [31] and n denotes the principal quantum number, l the orbital angular momentum, and j the total angular momentum. The reduced NMEs of (2) can now be calculated from [31]

$$(2_f^-\|\mathcal{O}_{1,2}^\pm\|0_i^+) = \sum_{ab}\frac{(a\|\mathcal{O}_{1,2}^\pm\|b)}{\sqrt{5}}(2_f^-\|[c_a^\dagger\tilde{c}_b]_2\|0_i^+), \tag{4}$$

where b and a denote the initial and final single-particle quantum numbers, 0_i^+ is the initial ground state in an even-even nucleus, and 2_f^- is a final 2^- state in an odd-odd nucleus.

The transition strength for a transition from the initial 0_i^+ ground state to the 2_f^- final state can be calculated from

$$S_{1,2}^\pm(f) = |(2_f^-\|\mathcal{O}_{1,2}^\pm\|0_i^+)|^2. \tag{5}$$

In the present work 0_i^+ corresponds to the ground state of a mother nucleus of $0\nu\beta\beta$ decay, and we need the (p,n) type strength $S_{1,2}^-(f)$ for the whole range of final states f, up to and beyond the IVSD $J^\pi = 2^-$ giant-resonance region, in order to be able to compare with the corresponding experimental data.

C. Two-neutrino double-beta decays

The half-life of the $2\nu\beta\beta$ decay can be written in the form

$$\left[t_{1/2}^{(2\nu)}(0_i^+ \to 0_f^+)\right]^{-1} = \left(g_{\text{A}}^{\text{eff}}\right)^4 G_{2\nu}|M^{(2\nu)}|^2, \tag{6}$$

where $g_{\text{A}}^{\text{eff}}$ is the effective value of the weak axial-vector coupling strength and $G_{2\nu}$ is a leptonic phase-space factor (in units of inverse years) as defined in Ref. [42] without the axial-vector coupling strength g_{A}. The initial and final ground states are denoted by 0_i^+ and 0_f^+, correspondingly. The Gamow-Teller NME involved in the equation is written in the pnQRPA formalism as

$$M^{(2\nu)} = \sum_{m,n}\frac{(0_f^+\|\sum_k t_k^-\,\sigma_k\|1_m^+)\langle 1_m^+|1_n^+\rangle(1_n^+\|\sum_k t_k^-\,\sigma_k\|0_i^+)}{D_m + 1} \tag{7}$$

for the $2\nu\beta^-\beta^-$ decays, with D_m being the energy denominator

$$D_m = \left(\tfrac{1}{2}\Delta + \tfrac{1}{2}[E(1_m^+) + \tilde{E}(1_m^+)] - M_i\right)/m_e, \tag{8}$$

where Δ is the nuclear mass difference between the initial and final 0^+ ground states, M_i the mass of the initial nucleus, m_e the electron rest mass, $\tilde{E}(1_m^+)$ is the (absolute) energy of the mth 1^+ state in a pnQRPA calculation based on the left-side ground state, and $E(1_m^+)$ the same for a calculation based on the right-side ground state. To do the calculations as accurately as possible, the difference $[E(1_m^+) + \tilde{E}(1_m^+)]/2 - M_i$ is adjusted to the experimental energy difference between the first 1^+ state in the intermediate nucleus and the ground state of the initial nucleus. The same is done in the calculations of the $0\nu\beta\beta$ NMEs. The quantity $\langle 1_m^+|1_n^+\rangle$ is the overlap between the two sets of 1^+ states and it can be written as

$$\langle 1_m^+|1_n^+\rangle = \sum_{pn}\left[X_{pn}^{1_m^+}\bar{X}_{pn}^{1_n^+} - Y_{pn}^{1_m^+}\bar{Y}_{pn}^{1_n^+}\right]. \tag{9}$$

The overlap factor matches the corresponding states in the two sets of states based on the left- and right-side even-even reference nuclei and makes the computed NMEs more stable. For deformed nuclei, and especially when the deformations of the mother and daughter nuclei are considerably different, the role of the overlap factor is important [43,44]. The quantities X and Y ($\bar{X}$ and $\bar{Y}$) denote the pnQRPA amplitudes which stem from the calculation based on the left-side (right-side) nucleus.

In principle, the expression in Eq. (7) should also contain a Fermi part, but our choice for the $g_{\text{pp}}^{T=1}$ parameter forces this contribution to zero, as will be explained in Sec. III A. This is justified since in the case of isospin symmetry, which is obeyed by the nuclear forces to a high degree, the ground states of the mother and daughter nuclei belong to different isospin multiplets and the Fermi contribution to the $2\nu\beta\beta$ NME should vanish, leaving the Gamow-Teller NME in Eq. (7) as the sole contributor to the $2\nu\beta\beta$ decay rate.

D. Neutrinoless double-beta decays

Assuming that the exchange of light Majorana neutrino dominates the $0\nu\beta\beta$ mechanisms, the half-life for a

ground-state-to-ground-state $0\nu\beta\beta$ transition can be written as

$$\left[t_{1/2}^{(0\nu)}(0_i^+ \to 0_f^+)\right]^{-1} = \left(g_{\rm A}^{\rm eff}\right)^4 G_{0\nu} |M^{(0\nu)}|^2 \left|\frac{\langle m_\nu\rangle}{m_e}\right|^2, \quad (10)$$

where $G_{0\nu}$ is a phase-space factor, cited in Ref. [42] in units of inverse years, for the final-state leptons defined here without the axial-vector coupling strength $g_{\rm A}$ [42] and $\langle m_\nu\rangle$ is the effective light-neutrino mass

$$\langle m_\nu\rangle = \sum_{j=\text{light}} \left(U_{ej}^l\right)^2 m_j \quad (11)$$

with m_j being the individual light-neutrino masses. Here the amplitudes U_{ej}^l are the components of the electron row of the neutrino-mixing matrix corresponding to the light sector.

The nuclear matrix element $M^{(0\nu)}$ in Eq. (10) is defined as

$$M^{(0\nu)} = M_{\rm GT}^{(0\nu)} - \left(\frac{g_{\rm V}}{g_{\rm A}^{\rm eff}}\right)^2 M_{\rm F}^{(0\nu)} + M_{\rm T}^{(0\nu)}, \quad (12)$$

where we adopt the CVC value $g_{\rm V} = 1.0$ for the weak vector coupling strength and the double Fermi, Gamow-Teller, and tensor nuclear matrix elements are defined for the $0\nu\beta^-\beta^-$ decays as

$$M_{\rm F}^{(0\nu)} = \sum_k \langle 0_f^+ \| \sum_{mn} h_{\rm F}(r_{mn}, E_k) t_m^- t_n^- \| 0_i^+\rangle, \quad (13)$$

$$M_{\rm GT}^{(0\nu)} = \sum_k \langle 0_f^+ \| \sum_{mn} h_{\rm GT}(r_{mn}, E_k)(\sigma_m \cdot \sigma_n) t_m^- t_n^- \| 0_i^+\rangle, \quad (14)$$

$$M_{\rm T}^{(0\nu)} = \sum_k \langle 0_f^+ \| \sum_{mn} h_{\rm T}(r_{mn}, E_k) S_{mn}^{\rm T} t_m^- t_n^- \| 0_i^+\rangle, \quad (15)$$

where the operator t_m^- is the isospin lowering operator (neutron to proton) for the nucleon m and the spin tensor operator is defined as

$$S_{mn}^{\rm T} = 3[(\sigma_m \cdot \hat{\mathbf{r}}_{mn})(\sigma_n \cdot \hat{\mathbf{r}}_{mn})] - \sigma_m \cdot \sigma_n. \quad (16)$$

The summation over k in Eqs. (13)–(15) runs over all the states of the intermediate odd-odd nucleus, $r_{mn} = |\mathbf{r}_m - \mathbf{r}_n|$ is the relative distance between the two decaying neutrons, labeled m and n, and $\hat{\mathbf{r}}_{mn} = (\mathbf{r}_m - \mathbf{r}_n)/r_{mn}$. As in the two-neutrino case the ground state of the initial even-even nucleus is denoted by 0_i^+ and the ground state of the final even-even nucleus is denoted by 0_f^+. Expressions for the neutrino potentials $h_K(r_{mn}, E_k)$, $K = \text{F, GT, T}$ are given in Ref. [29].

The nuclear matrix elements can be written in the pnQRPA framework as

$$M_K^{(0\nu)} = \sum_{J^\pi, k_1, k_2, J'} \sum_{pp'nn'} (-1)^{j_n + j_{p'} + J + J'} \sqrt{2J'+1} \times \begin{Bmatrix} j_p & j_n & J \\ j_{n'} & j_{p'} & J' \end{Bmatrix} (pp' : J' \| \mathcal{O}_K \| nn' : J') \times \langle 0_f^+ \| [c_{p'}^\dagger \tilde{c}_{n'}]_J \| J_{k_1}^\pi \rangle \langle J_{k_1}^\pi | J_{k_2}^\pi \rangle \langle J_{k_2}^\pi \| [c_p^\dagger \tilde{c}_n]_J \| 0_i^+ \rangle, \quad (17)$$

where k_1 and k_2 label the different pnQRPA solutions for a given multipole J^π. The operators $\mathcal{O}_K$ inside the two-particle matrix element correspond to the ones of Eqs. (13), (14), and (15), and they can be written as

$$\mathcal{O}_{\rm F} = h_{\rm F}(r, E_k)[f_{\rm CD}(r)]^2, \quad (18)$$

$$\mathcal{O}_{\rm GT} = h_{\rm GT}(r, E_k)[f_{\rm CD}(r)]^2 \, \sigma_1 \cdot \sigma_2, \quad (19)$$

$$\mathcal{O}_{\rm T} = h_{\rm T}(r, E_k)[f_{\rm CD}(r)]^2 S_{12}^{\rm T}, \quad (20)$$

where $S_{12}^{\rm T}$ is the tensor operator of Eq. (16) and $r = |\mathbf{r}_1 - \mathbf{r}_2|$ is the distance between the participating nucleons. The energy E_k is the average of the kth eigenvalues of the pnQRPA calculations based on the initial and final nuclei of the decay, and the overlap factor $\langle J_{k_1}^\pi | J_{k_2}^\pi \rangle$ in Eq. (17) is the one of Eq. (9). It has an important role for deformed nuclei, especially when the deformations of the mother and daughter nuclei are considerably different. The factor $f_{\rm CD}(r)$ takes into account the nucleon-nucleon short-range correlations (SRC) [32,45] and here we use the CD-Bonn form [46] with the parametrization

$$f_{\rm CD}(r) = 1 - 0.46 e^{-(1.52/\text{fm}^2) r^2}[1 - (1.88/\text{fm}^2) r^2]. \quad (21)$$

In the pnQRPA the state of Eq. (1) leads to the transition densities

$$\langle 0_f^+ \| [c_{p'}^\dagger \tilde{c}_{n'}]_J \| J_{k_1}^\pi \rangle = \hat{J}\left[\bar{v}_{p'} \bar{u}_{n'} \bar{X}_{p'n'}^{J^\pi k_1} + \bar{u}_{p'} \bar{v}_{n'} \bar{Y}_{p'n'}^{J^\pi k_1}\right], \quad (22)$$

$$\langle J_{k_2}^\pi \| [c_p^\dagger \tilde{c}_n]_J \| 0_i^+ \rangle = \hat{J}\left[u_p v_n X_{pn}^{J^\pi k_2} + v_p u_n Y_{pn}^{J^\pi k_2}\right], \quad (23)$$

where v ($\bar{v}$) and u ($\bar{u}$) correspond to the BCS occupation and vacancy amplitudes of the initial (final) even-even nucleus. The amplitudes X and Y ($\bar{X}$ and $\bar{Y}$) emerge from the pnQRPA calculation based on the initial (final) nucleus of the double-beta decay. Equation (17) does not include the overlap between the initial and final BCS states that can be rather important, according to the recent study by Fang *et al.* based on the deformed QRPA formalism [47]. In this work it was found that the $0\nu\beta\beta$ NMEs were reduced by as much as 30–60% in comparison with the spherical formalism, mainly due to the BCS overlap factors and partly due to the deformation. According to the discussion in Ref. [47], the BCS factors could cause a large (as large as 60%) decrease to the calculated NMEs, if the neutron or proton number is close to a magic number (as for ^{116}Cd and ^{136}Xe), and a milder (≈20–30%) decrease in the other cases. In a purely spherical pnQRPA approach it is expected that these changes in the NMEs constitute an upper limit. In particular one has to be careful in using the BCS overlap for the semimagic nuclei where the BCS approach does not produce a pairing gap, and some higher-order approach, like the Lipkin-Nogami approach [31], would be better.

III. RESULTS AND DISCUSSION

In this section we present and discuss the results of our studies. In the calculations we use two slightly different sets of single-particle bases, and we also compare our results with the numbers obtained in an earlier study of Hyvärinen *et al.* [29] of the same $0\nu\beta\beta$ transitions.

A. Determination of model parameters

Here we adopt the single-particle bases used in the isovector spin-multipole calculations of [35] discussed already in

Sec. II A. We decompose each isobaric triplet with mass number A to "left-side" even-even (A, N, Z), "right-side" even-even $(A, N-2, Z+2)$ and "intermediate" odd-odd $(A, N-1, Z+1)$ nuclei and construct the spectra of J^π excitations in the intermediate odd-odd nuclei, applying the pnQRPA formalism [31,38,39] to the left- and right-side even-even nuclei. In this way one obtains two sets of energies and wave functions for each J^π state. The residual Hamiltonian for the pnQRPA includes particle-hole and particle-particle components. The particle-hole contribution is proportional to the particle-hole matrix elements $g_{\rm ph}\langle pn^{-1}; J^\pi|V|p'n'^{-1}; J^\pi\rangle$, where J^π is the multipole of the states in the intermediate odd-odd nucleus, and the particle-particle contribution is proportional to the two-body matrix elements $g_{\rm pp}\langle pn; J^\pi|V|p'n'; J^\pi\rangle$. Here $g_{\rm ph}$ and $g_{\rm pp}$ are the particle-hole and particle-particle renormalization factors correspondingly.

Traditionally the $g_{\rm ph}$ parameter is fixed by fitting the centroid of the Gamow-Teller resonance (GTR) in the 1^+ channel of the calculations [1,38,39,48,49]. This same $g_{\rm ph}$ is then used for all multipoles J^π. We use this method as a starting point (we call this Model 1), but explore how the particle-hole parameter $g_{\rm ph}(2^-)$ changes the values of the $0\nu\beta\beta$ NMEs by fitting the $J^\pi = 2^-$ channel separately (Model 2) and by using the $g_{\rm ph}(2^-)$ parameter for all channels excluding the 1^+ channel (Model 3). We adjust the $g_{\rm ph}(1^+)$ and $g_{\rm ph}(2^-)$ parameters to the available data on Gamow-Teller [50–53] and isovector spin-dipole giant-resonance energies [53–58].

The GT and IVSD strength distributions were studied at RCNP, Osaka University, through high-resolution (^{3}He,t) charge-exchange reactions. Significant GT and IVSD strengths are found as broad giant resonances around 12 and 20 MeV, and the widths are around 5 and 10 MeV, respectively. In fact, the IVSD resonance was first discussed in Ref. [59] to account for the reduction of the low-lying SD β NMEs. We adjust the $g_{\rm ph}(2^-)$ parameter to the available data on the giant resonance energies. The data for different nuclei are: ^{76}Ge [53], ^{96}Zr [54], ^{100}Mo [55], ^{116}Cd [56], ^{128}Te [57], ^{130}Te [57], and ^{136}Xe [58]. The GTR and IVSD energies for the DBD nuclei of current interest are expressed approximately as

$$\begin{aligned} E(\mathrm{GT}) &\approx 9 + 0.4T_Z \text{ MeV}, \\ E(\mathrm{SD}) &\approx 16.5 + 0.4T_Z \text{ MeV}, \end{aligned} \tag{24}$$

where $T_Z = \frac{1}{2}(N-Z)$. The uncertainties of the GT and IVSD energies are around ± 0.5 and 1 MeV, respectively. The $g_{\rm ph}$ values adjusted in this way are presented in Table II, together with the values of the GTR and IVSD giant-resonance centroids obtained from Eq. (24). For $A = 96$ we use the measured centroid, as the linear fits of (24) do not reproduce the measured values well. It is seen in Table II that the $g_{\rm ph}$ values vary by 20–30% depending on the basis (WS/sp) and the type of GR (GT/SD).

The $g_{\rm pp}$ parameter has usually been adjusted by fitting this value to the measured $2\nu\beta\beta$-decay half-life [32–34,60,61], to the log ft values of β decays [62,63], or to both β and $2\nu\beta\beta$ decays [64,65]. In this work, we adopt an improved method introduced in Ref. [28] and later used in Ref. [29], where we decompose the pnQRPA NMEs into isoscalar ($T = 0$) and isovector ($T = 1$) parts and then adjust the parameters

TABLE II. Parameters of the pnQRPA calculations for various $0\nu\beta\beta$ decaying nuclei. Column 2 indicates the basis that was used in the calculations. Columns 3 and 4 list the experimental centroid energies of the IVSD $J^\pi = 2^-$ and GTR $J^\pi = 1^+$ resonances. The last two columns list the values of the particle-hole parameters adjusted to the locations of the IVSD resonance and the GTR.

Nucleus	Basis	$E(\mathrm{SD}2^-)$ (MeV)	$E(\mathrm{GT})$ (MeV)	$g_{\rm ph}(2^-)$	$g_{\rm ph}(1^+)$
^{76}Ge	WS	18.9 ± 1.0	11.4 ± 0.5	0.9 ± 0.2	1.24 ± 0.13
	sp			1.2 ± 0.3	1.03 ± 0.13
^{96}Zr	sp	22 ± 1.0	12.7 ± 0.5	0.8 ± 0.2	0.84 ± 0.09
^{100}Mo	sp	19.7 ± 1.0	12.2 ± 0.5	1.0 ± 0.2	1.19 ± 0.08
^{116}Cd	WS	20.5 ± 1.0	13.0 ± 0.5	1.07 ± 0.09	0.85 ± 0.13
^{128}Te	WS	21.3 ± 1.0	13.8 ± 0.5	1.7 ± 0.2	1.64 ± 0.08
	sp			1.9 ± 0.2	1.40 ± 0.09
^{130}Te	WS	21.7 ± 1.0	14.2 ± 0.5	1.7 ± 0.2	1.58 ± 0.08
	sp			1.9 ± 0.2	1.36 ± 0.09
^{136}Xe	WS	22.1 ± 1.0	14.6 ± 0.5	1.0 ± 0.2	1.36 ± 0.07
	sp			0.9 ± 0.2	1.18 ± 0.08

$g_{\rm pp}^{T=0}$ and $g_{\rm pp}^{T=1}$ independently. The particle-particle parts of the pnQRPA matrices are divided into isoscalar ($T = 0$) and isovector ($T = 1$) parts by the decomposition

$$\begin{aligned} &g_{\rm pp}\langle pn; J^\pi|V|p'n'; J^\pi\rangle \\ &\quad\rightarrow g_{\rm pp}^{T=1}\langle pn; J^\pi; T=1|V|p'n'; J^\pi; T=1\rangle \\ &\qquad + g_{\rm pp}^{T=0}\langle pn; J^\pi; T=0|V|p'n'; J^\pi; T=0\rangle. \end{aligned} \tag{25}$$

The isovector parameter $g_{\rm pp}^{T=1}$ is adjusted so that the Fermi $2\nu\beta\beta$ NME vanishes, and thus the isospin symmetry is partially restored. Then we independently vary the isoscalar parameter $g_{\rm pp}^{T=0}$ such that it reproduces the calculated matrix element corresponding to the measured $2\nu\beta\beta$ half-life and a (moderately) quenched effective value $g_{\rm A}^{\rm eff} = 1.0$ of the axial-vector coupling strength. These values are determined for each mass number separately, and the obtained parameters are adopted for all multipoles in both the left- and right-side even-even nuclei. We list the obtained values in Table III. The $g_{\rm pp}^{T=0,1}$ values depend on the $g_{\rm ph}$ value only weakly: The variation in

TABLE III. The $g_{\rm pp}$ parameters used in the present calculations for the isoscalar (column 3) and the isovector (column 4) interaction.

Nucleus	Basis	$g_{\rm pp}^{T=0}(g_{\rm A} \approx 1.00$–$1.27)$	$g_{\rm pp}^{T=1}$
^{76}Ge	WS	0.80	0.99
	sp	0.83	0.96
^{96}Zr	sp	0.83	0.93
^{100}Mo	sp	0.87	0.91
^{116}Cd	WS	0.82	0.82
^{128}Te	WS	0.73	0.94
	sp	0.745	0.87
^{130}Te	WS	0.74	0.95
	sp	0.73	0.86
^{136}Xe	WS	0.64	0.98
	sp	0.67	0.87

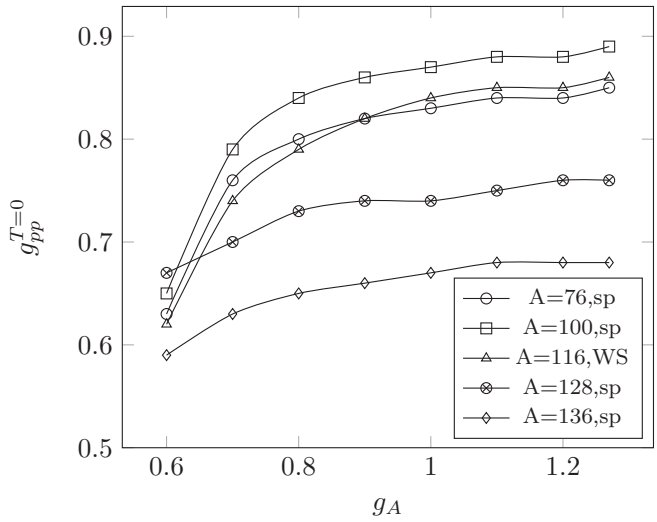

FIG. 1. Values of the particle-particle parameter $g_{pp}^{T=0}$ as functions of g_A for a representative set of bases and different nuclei.

the range of the g_{ph} values of Table II is only about 1–5% for each nucleus. Since the impact of the variation on the NME values in negligible, the g_{pp} values obtained with $g_{ph}(1^+)$ were adopted. The bare value $g_A^{bare} = 1.27$ was also tested in the determination of the $g_{pp}^{T=0}$ parameters, but the parameter values obtained this way differed only by 1–3% from those obtained with $g_A^{eff} = 1.0$ (see Fig. 1) so we do not list them separately for $g_A^{bare} = 1.27$. It seems that in the considered large basis sets the behavior of g_{pp} as a function of g_A is rather flat for values larger than 1, and only for the smaller g_A values do the variations in the g_{pp} values set in. Hence, the $2\nu\beta\beta$ nuclear matrix element $M^{(2\nu)}$ is strongly dependent on the $g_{pp}^{T=0}$ value (see Fig. 2). As a result, the values of the NMEs $M_{GT}^{(0\nu)}$, $M_F^{(0\nu)}$, and $M_T^{(0\nu)}$ are altered mildly in the range $g_A \approx 1.00$–1.27, resulting in about 10–20% changes in the total NMEs $M^{(0\nu)}$ as in Ref.

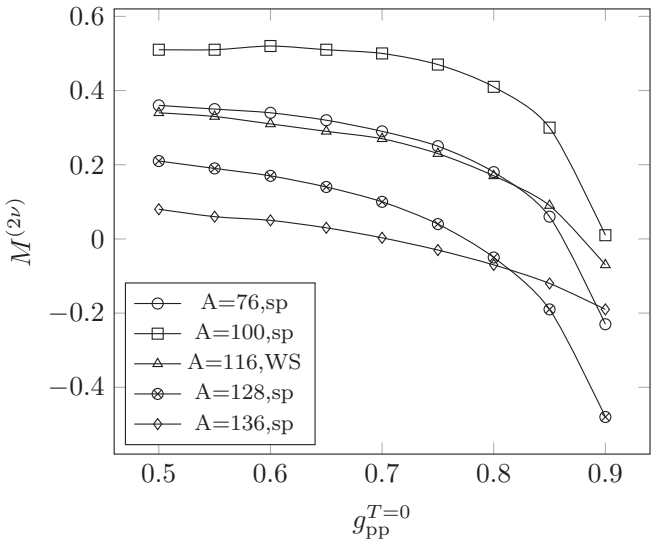

FIG. 2. Values of the $2\nu\beta\beta$ nuclear matrix element as functions of $g_{pp}^{T=0}$ for a representative set of bases and different nuclei.

TABLE IV. IAS energies calculated using $g_{ph}(1^+)$ of Table II and $g_{pp}^{T=0,1}$ of Table III. The corresponding experimental IAS energies are listed in the last column.

Nucleus	$E(\text{IAS})_{sp}$ (MeV)	$E(\text{IAS})_{WS}$ (MeV)	$E_{fit}(\text{IAS})$ (MeV)
^{76}Ge	6.5	7.0	8.6
^{96}Zr	5.8		9.8
^{100}Mo	9.5		9.8
^{116}Cd		9.8	11.0
^{128}Te	11.0	11.9	12.2
^{130}Te	10.6	11.4	12.8
^{136}Xe	10.1	10.5	13.4

[29], and we adopt the effective value $g_A^{eff} = 1.0$ in the present calculations.

The IAS (isobaric analog state) energies calculated using the $g_{ph}(1^+)$ values of Table II and $g_{pp}^{T=0,1}$ values of Table III are presented in Table IV. From the results of [53–59] we can derive the following expression for the experimental IAS locations for the DBD nuclei of current interest:

$$E_{fit}(\text{IAS}) = 5 + 0.6T_Z \text{ MeV}, \tag{26}$$

where $T_Z = \frac{1}{2}(N - Z)$. These values are presented in Table IV for comparison. As can be seen in the table the computed locations of the IAS are too low in comparison with the experimental locations. The difference between the computed and the experimental locations varies between 1.2 and 4 MeV, except for the cases $A = 100$ and 128 (sp basis), for which the differences are less than 0.5 MeV. The sum rule $S_- - S_+ = N - Z$, S_- [S_+] being the total Fermi strength in the (p, n) [(n, p)] direction, is exactly fulfilled in our calculations. The discrepancy in the computed IAS energies is typical of pnQRPA calculations which are not self-consistent, i.e., the mean field is not determined by the same Hamiltonian as the excited states. In self-consistent calculations the situation is improved and the discrepancies reach typically a level below 1 MeV, the computed energies of the IAS being still below the measured ones (see, e.g., [66]).

B. IVSD $J^\pi = 2^-$ strength functions

The $J^\pi = 2^-$ strength functions were calculated in the bare Woods-Saxon (WS) bases, as well as in the slightly modified single-particle (sp) bases. Two different g_{ph} values were adopted: one was obtained by adjusting it to the measured location of the Gamow-Teller (GT) giant resonance, and the other was obtained by adjusting it to the measured location of the IVSD $J^\pi = 2^-$ giant resonance (see Sec. III A). The resulting strength functions for mass numbers $A = 76$, 100, 116, and 128 are presented in Figs. 3–6. In the figures we use Lorentzian folding with a peak width of 0.5 MeV [35].

As we can see in Fig. 3, for $A = 76$ the large, about 30%, deviation between the values of $g_{ph}(1^+)$ and $g_{ph}(2^-)$ (see Table II) results in large deviations between the strength functions calculated using the WS basis. On the other hand, for the sp basis the difference between the different g_{ph} values is

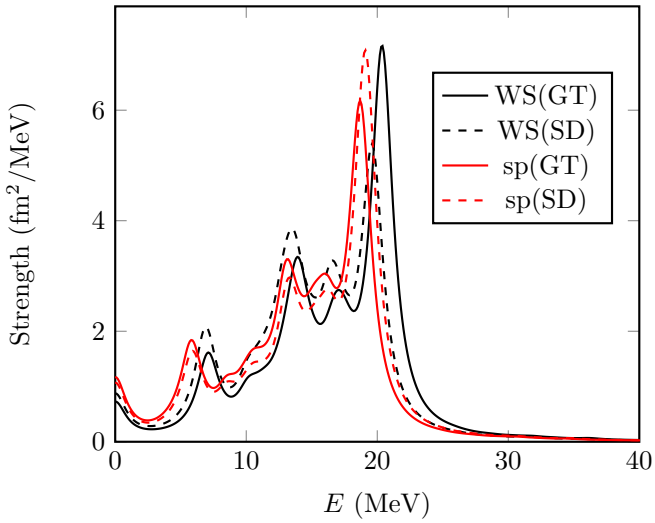

FIG. 3. Isovector spin-dipole $J^\pi = 2^-$ strength functions for $A = 76$ calculated using either a Woods-Saxon (WS) or a modified Woods-Saxon (sp) single-particle basis, and $g_{\rm ph}$ values obtained by fitting to the location of either the Gamow-Teller (GT) or the IVSD $J^\pi = 2^-$ giant resonance.

smaller, which leads to smaller deviations between the strength functions.

From Fig. 4 we see that for $A = 100$ the moderate, about 15%, deviation between the $g_{\rm ph}$values (see Table II) leads to moderate differences between the calculated strength functions. From Fig. 5, in turn, we see that large deviations between the $g_{\rm ph}$ values lead to large deviations between the strength functions.

As can be seen in Fig. 6, for $A = 128$ the large, about 30%, deviations in $g_{\rm ph}$ values lead to large deviations in the strength functions calculated using the sp basis. The small, about 4%, difference between the $g_{\rm ph}$ values, on the other hand, leads to small differences in the strength functions calculated using the WS basis.

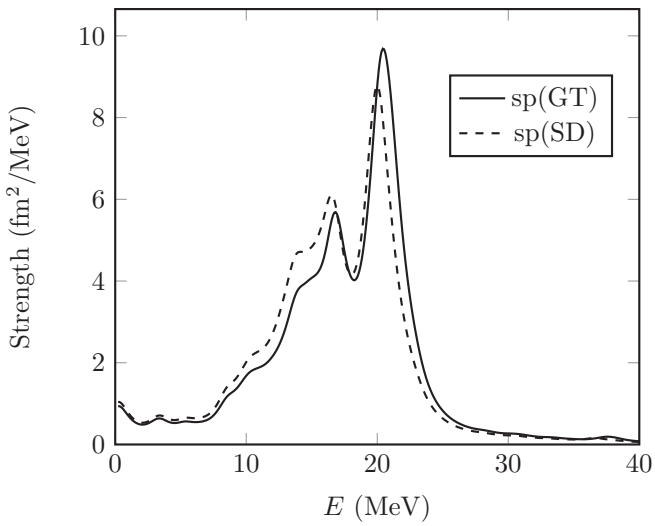

FIG. 4. The same as Fig. 3 for $A = 100$.

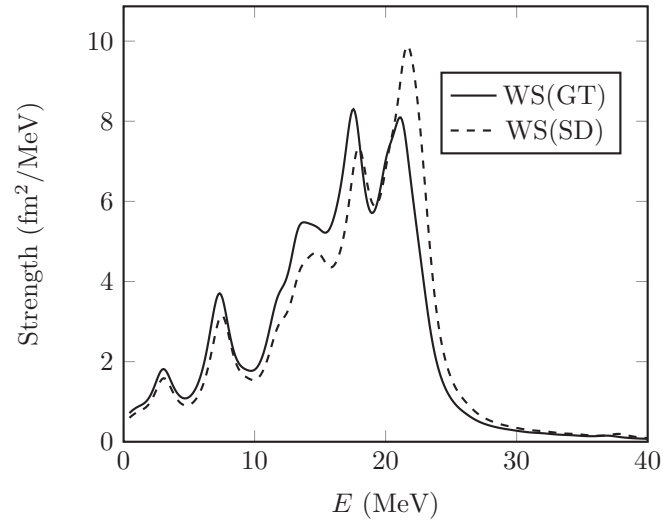

FIG. 5. The same as Fig. 3 for $A = 116$.

For $A = 96$ the strength functions were almost identical, so the corresponding spectra are not presented here. The cases $A = 130$ and 136 were almost identical with $A = 128$, with slightly more moderate deviations between the different spectra, so the figures are omitted here.

C. Matrix elements for neutrinoless $\beta\beta$ decay

We present our final results for the nuclear matrix elements ($M^{(0\nu)}$) of the light-Majorana-mediated neutrinoless $\beta\beta$ decay using the two sets of single-particle bases discussed in Sec. II A. Furthermore, we investigate the impact of using the $g_{\rm ph}(2^-)$ value in the evaluation of the $0\nu\beta\beta$ NME by using three different methods. That is, for both sets of bases we compute $M^{(0\nu)}$ [Eq. (12)] first by using the common parameter $g_{\rm ph} = g_{\rm ph}(1^+)$ for each multipole (Model 1), then change the $g_{\rm ph}$ value into $g_{\rm ph}(2^-)$ for the multipole $J^\pi = 2^-$, and keep $g_{\rm ph} = g_{\rm ph}(1^+)$ for the other multipoles (Model 2). Furthermore, we

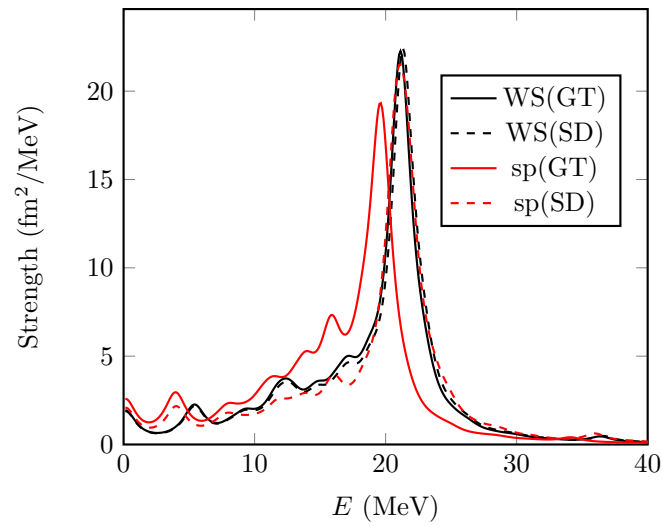

FIG. 6. The same as Fig. 3 for $A = 128$.

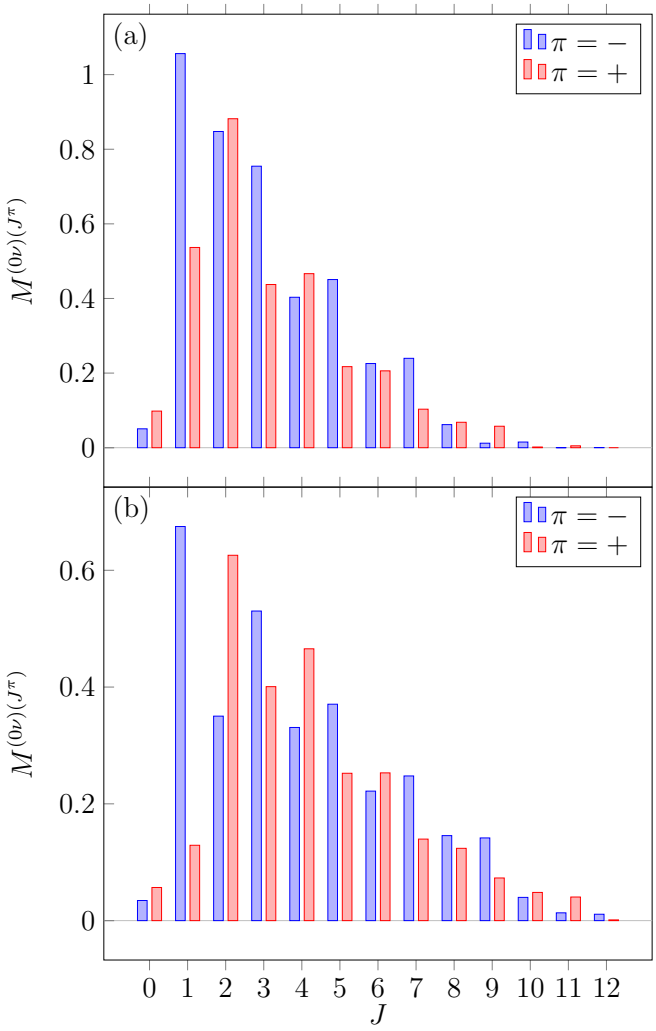

FIG. 7. Multipole decomposition of the total $0\nu\beta\beta$ matrix element $M^{(0\nu)}$ of (a) ^{76}Ge (b) ^{128}Te.

perform the calculations using $g_{\rm ph}(1^+)$ for the 1^+ channel and $g_{\rm ph}(J^\pi) = g_{\rm ph}(2^-)$ for $J^\pi \neq 1^+$ (Model 3). The $g_{\rm pp}^{T=0,1}$ values of Table III are used for each multipole. We adopt the effective axial-vector coupling $g_{\rm A}^{\rm eff} = 1.00$ for our $0\nu\beta\beta$ NME calculations. We use the effective $g_{\rm A}$ to incorporate the nuclear medium and non-nucleonic correlations, but we use $g_{\rm V} = 1.0$ on the basis of the CVC.

The relative importance of the 2^- contributions in the $0\nu\beta\beta$ NMEs has been illustrated in Fig. 7. For a medium-heavy nucleus, like ^{76}Ge [panel (a) of Fig. 7)], the contributions from the 2^- states can be considerable. For a heavier nucleus, like ^{128}Te [panel (b) of Fig. 7], the contribution is not that conspicuous. Nevertheless, it is worth studying the effect of the spin-dipole states on the values of the $0\nu\beta\beta$ NMEs.

We present our final NMEs of Eq. (12) in Tables V and VI, and compare them with the results of Hyvärinen *et al.* [29] for $g_{\rm A}^{\rm eff} = 1.00$. In Ref. [29] smaller single-particle bases were used, i.e., the orbitals $1p$–$0f$–$2s$–$1d$–$0g$–$0h_{11/2}$ for the $A = 76, 82$ systems, the orbitals $1p$–$0f$–$2s$–$1d$–$0g$–$0h$ for the $A = 96, 100$ systems, and the orbitals $1p$–$0f$–$2s$–$1d$–$0g$–$2p$–$1f$–$0h$ for the $A = 116, 128, 130, 136$ systems. The same orbitals were used for both neutrons and protons. The $g_{\rm pp}^{T=0,1}$ parameters were determined in the same manner as in the present study, and the $g_{\rm ph}$ parameter was adjusted to the GTR in the traditional way.

If we compare the content of Tables II and V with the differences shown in Fig. 8 and with the IVSD $J^\pi = 2^-$ strength functions in Figs. 3–6, we can draw the following conclusions.

***A* = 76**: There is a large, about 30%, difference between the IVSD- and GT-determined $g_{\rm ph}$ values for the WS basis. This is reflected as a large difference in both the strength functions, Fig. 3, and $0\nu\beta\beta$ NMEs, Table V. Increasing the impact of $g_{\rm ph}(2^-)$ on the NMEs (Model 3) increases the difference even more. For the sp basis the differences are smaller for all quantities and, in particular, the deviations from the NME computed in the smaller single-particle space [29] are on the percent level.

***A* = 96**: The deviations in the $g_{\rm ph}$ values, and $0\nu\beta\beta$ NMEs are small, at the few-percent level. However, there is a notable deviation from the small-basis $0\nu\beta\beta$ NME [29].

***A* = 100**: The adjusted $g_{\rm ph}$ values differ by some 20%, and also the strength functions (cf. Fig. 4) change correspondingly. There is a negligible difference in the values of the $0\nu\beta\beta$ NMEs between Model 1 and Model 2, but a notable difference when going to Model 3. There is also a notable deviation from the NME value obtained in the smaller basis [29].

***A* = 116**: The determined $g_{\rm ph}$ values deviate by some 20%, producing slight differences in the strength functions, as seen in Fig. 5. As a result, the values of the $0\nu\beta\beta$ NMEs do not differ from each other between Model 1 and Model 2, and only slightly when going to Model 3. However, there is a notable deviation from the one computed in the smaller basis [29].

***A* = 128**: There are notable, about 30%, deviations in the $g_{\rm ph}$ values for the sp basis and this is reflected in the deviations in the strength functions, Fig. 6, for the sp-basis based calculations. Deviations in the values of the $0\nu\beta\beta$ NMEs between Model 1 and Model 2 are moderate, less than a percent within a given basis, but there are few-percent deviations when going from the WS-computed to the sp-computed NMEs. The sp-computed NMEs of Model 1 and Model 2 are consistent with the one produced in the smaller basis [29]. However, using Model 3 causes again some 10% deviations from the small-basis NME when using the sp basis.

***A* = 130**: The situation is similar to the $A = 128$ case, except that all the sp-computed $0\nu\beta\beta$ NMEs deviate by 10–20% from that computed in the smaller basis [29].

***A* = 136**: There are 20–30% differences in the $g_{\rm ph}$ values for both bases but the differences in the strength functions are moderate. Except for the NME computed in Model 3 in the sp basis, there are only some 10% differences in the values of the WS-computed and the sp-computed $0\nu\beta\beta$ NMEs, and less than 7% deviations from the NME obtained in the smaller basis [29].

Table V shows that the adoption of the IVSD $J^\pi = 2^-$-fitted value of $g_{\rm ph}$ for the 2^- channel of the $0\nu\beta\beta$ NMEs (Model 2) affects the NMEs negligibly for all of the cases (blue dots

TABLE V. Values of the $0\nu\beta\beta$ NMEs for $g_A^{\rm eff} = 1.00$. The first column indicates the transition, the second column the basis used in the calculation, and the third one the model adopted for the $g_{\rm ph}$ values. Model 1: $g_{\rm ph}(1^+)$ used for all J^π; Model 2: $g_{\rm ph}(2^-)$ used for $J^\pi = 2^-$, for the rest $g_{\rm ph}(1^+)$ is used; Model 3: $g_{\rm ph}(1^+)$ used for $J^\pi = 1^+$, for the rest $g_{\rm ph}(2^-)$ is used. The columns 4 to 6 show the decomposition of the total NMEs (column 7) in terms of the Fermi, Gamow-Teller, and tensor contributions. The last row for each transition corresponds to the earlier calculations performed in Ref. [29]. The quoted errors only take into account uncertainties due to the strength of the particle-hole interaction.

Nuclear transition	Basis	Model	$M_{\rm F}^{(0\nu)}$	$M_{\rm GT}^{(0\nu)}$	$M_{\rm T}^{(0\nu)}$	$M^{(0\nu)}$
^{76}Ge $\longrightarrow$ ^{76}Se	WS	1	-1.76 ± 0.06	5.4 ± 0.2	-0.356 ± 0.013	6.8 ± 0.3
	WS	2	-1.76 ± 0.05	5.5 ± 0.2	-0.357 ± 0.012	6.9 ± 0.3
	WS	3	-1.95 ± 0.11	5.8 ± 0.3	-0.31 ± 0.03	7.4 ± 0.4
	sp	1	-1.99 ± 0.08	5.3 ± 0.2	-0.390 ± 0.015	6.9 ± 0.3
	sp	2	-1.99 ± 0.08	5.2 ± 0.2	-0.389 ± 0.014	6.8 ± 0.3
	sp	3	-1.90 ± 0.13	5.1 ± 0.3	-0.41 ± 0.03	6.6 ± 0.4
	sp, small [29]	1	-1.74	5.07	-0.28	6.54
^{96}Zr $\longrightarrow$ ^{96}Mo	sp	1	-1.64 ± 0.06	3.95 ± 0.12	-0.254 ± 0.014	5.3 ± 0.2
	sp	2	-1.64 ± 0.06	3.97 ± 0.14	-0.255 ± 0.013	5.3 ± 0.2
	sp	3	-1.68 ± 0.13	4.0 ± 0.3	-0.24 ± 0.04	5.5 ± 0.4
	sp, small [29]	1	-1.44	3.26	-0.23	4.47
^{100}Mo $\longrightarrow$ ^{100}Ru	sp	1	-2.30 ± 0.05	3.74 ± 0.04	-0.500 ± 0.010	5.54 ± 0.10
	sp	2	-2.30 ± 0.05	3.76 ± 0.05	-0.503 ± 0.009	5.55 ± 0.11
	sp	3	-2.43 ± 0.15	3.9 ± 0.2	-0.47 ± 0.03	5.9 ± 0.4
	sp, small [29]	1	-1.63	3.62	-0.27	4.98
^{116}Cd $\longrightarrow$ ^{116}Sn	WS	1	-1.76 ± 0.07	4.11 ± 0.12	-0.171 ± 0.012	5.7 ± 0.2
	WS	2	-1.76 ± 0.07	4.08 ± 0.11	-0.168 ± 0.013	5.7 ± 0.2
	WS	3	-1.64 ± 0.05	3.94 ± 0.08	-0.191 ± 0.008	5.39 ± 0.13
	WS, small [29]	1	-1.50	3.61	-0.17	4.93
^{128}Te $\longrightarrow$ ^{128}Xe	WS	1	-1.65 ± 0.04	4.68 ± 0.08	-0.523 ± 0.010	5.81 ± 0.12
	WS	2	-1.65 ± 0.04	4.67 ± 0.10	-0.523 ± 0.009	5.81 ± 0.14
	WS	3	-1.64 ± 0.08	4.7 ± 0.2	-0.53 ± 0.03	5.8 ± 0.3
	sp	1	-1.77 ± 0.05	4.27 ± 0.09	-0.523 ± 0.011	5.52 ± 0.15
	sp	2	-1.77 ± 0.05	4.22 ± 0.09	-0.519 ± 0.011	5.47 ± 0.15
	sp	3	-1.55 ± 0.08	3.89 ± 0.13	-0.59 ± 0.03	4.9 ± 0.3
	sp, small [29]	1	-1.78	4.40	-0.43	5.74
^{130}Te $\longrightarrow$ ^{130}Xe	WS	1	-1.46 ± 0.03	4.04 ± 0.07	-0.468 ± 0.008	5.03 ± 0.10
	WS	2	-1.46 ± 0.03	4.03 ± 0.08	-0.468 ± 0.007	5.02 ± 0.12
	WS	3	-1.42 ± 0.07	3.97 ± 0.15	-0.48 ± 0.03	4.9 ± 0.3
	sp	1	-1.53 ± 0.04	3.70 ± 0.08	-0.460 ± 0.009	4.77 ± 0.12
	sp	2	-1.53 ± 0.04	3.65 ± 0.08	-0.456 ± 0.009	4.72 ± 0.12
	sp	3	-1.30 ± 0.06	3.31 ± 0.09	-0.53 ± 0.02	4.1 ± 0.2
	sp, small [29]	1	-1.52	4.12	-0.38	5.27
^{136}Xe $\longrightarrow$ ^{136}Ba	WS	1	-0.683 ± 0.010	2.83 ± 0.06	-0.227 ± 0.004	3.28 ± 0.07
	WS	2	-0.683 ± 0.010	2.90 ± 0.09	-0.229 ± 0.003	3.35 ± 0.10
	WS	3	-0.683 ± 0.010	2.93 ± 0.10	-0.231 ± 0.003	3.38 ± 0.12
	sp	1	-1.01 ± 0.03	2.96 ± 0.06	-0.249 ± 0.005	3.72 ± 0.09
	sp	2	-1.01 ± 0.03	3.01 ± 0.08	-0.251 ± 0.005	3.76 ± 0.10
	sp	3	-1.12 ± 0.06	3.21 ± 0.15	-0.220 ± 0.014	4.1 ± 0.3
	sp, small [29]	1	-0.89	2.82	-0.22	3.50

in Fig. 8). Adoption of $g_{\rm ph}(2^-)$ for all multipoles $J^\pi \neq 1^+$ (Model 3), however, causes larger deviations in all cases (red squares and open triangles in Fig. 8).

The results obtained in the WS bases deviate from those obtained in the sp bases by about 12% in the case of $A = 136$, and by less than 10% in the other cases for Model 1 and Model 2, as seen in Fig. 9, blue dots and red squares. However, for Model 3 the differences between the different single-particle bases are 15–21% for $A = 128, 130, 136$ and about 11% for $A = 76$. Hence, the features of the single-particle valence spaces affect notably the values of the NMEs.

The present results are summarized in Table VI where we quote the combined no-core $0\nu\beta\beta$ NMEs of Model 2 and Model 3. Comparing the NME values of Table VI with the NMEs of [29] shows that the present results deviate from those obtained in the smaller basis [29] by less than 4% for $A = 76, 136$, and about 10–18% for the rest (see also the black asterisks in Fig. 8). Hence, the numbers of Table VI indicate that the NME results of Hyvärinen *et al.* [29] deviate by at most 18% from the present results, the differences emerging from variations in the nuclear mean field, size of the single-particle valence space, and variations in the value of $g_{\rm ph}$.

TABLE VI. Computed no-core nuclear matrix elements for $g_A^{\text{eff}} = 1.00$ (column 2); combined results of Model 2 and Model 3 are adopted. Given are also the single-particle bases (column 3) and the nuclear-structure coefficients of Eq. (27) (column 4). The phase-space factors are taken from [42].

Nuclear transition	$0\nu\beta\beta$ NME	Basis	$C^{(0\nu)}$
$^{76}\text{Ge} \longrightarrow {}^{76}\text{Se}$	6.7 ± 0.3	sp	0.25 ± 0.03
$^{96}\text{Zr} \longrightarrow {}^{96}\text{Mo}$	5.4 ± 0.3	sp	0.044 ± 0.005
$^{100}\text{Mo} \longrightarrow {}^{100}\text{Ru}$	5.7 ± 0.3	sp	0.050 ± 0.006
$^{116}\text{Cd} \longrightarrow {}^{116}\text{Sn}$	5.55 ± 0.12	WS	0.051 ± 0.003
$^{128}\text{Te} \longrightarrow {}^{128}\text{Xe}$	5.2 ± 0.2	sp	1.64 ± 0.13
$^{130}\text{Te} \longrightarrow {}^{130}\text{Xe}$	4.41 ± 0.12	sp	0.094 ± 0.006
$^{136}\text{Xe} \longrightarrow {}^{136}\text{Ba}$	3.9 ± 0.2	sp	0.118 ± 0.013

The expression for the half-life, Eq. (10), can be written in an easily usable form,

$$t_{1/2}^{(0\nu)}(0_i^+ \longrightarrow 0_f^+) = \frac{C^{(0\nu)}}{(|\langle m_\nu \rangle|[\text{eV}])^2} \times 10^{25}\ \text{yr}, \qquad (27)$$

where the effective electron neutrino mass is given in eV. From this expression it is easy to derive the values of the half-lives once the value of the neutrino mass is known. We list the nuclear-structure coefficients $C^{(0\nu)}$, together with the adopted NMEs, in Table VI.

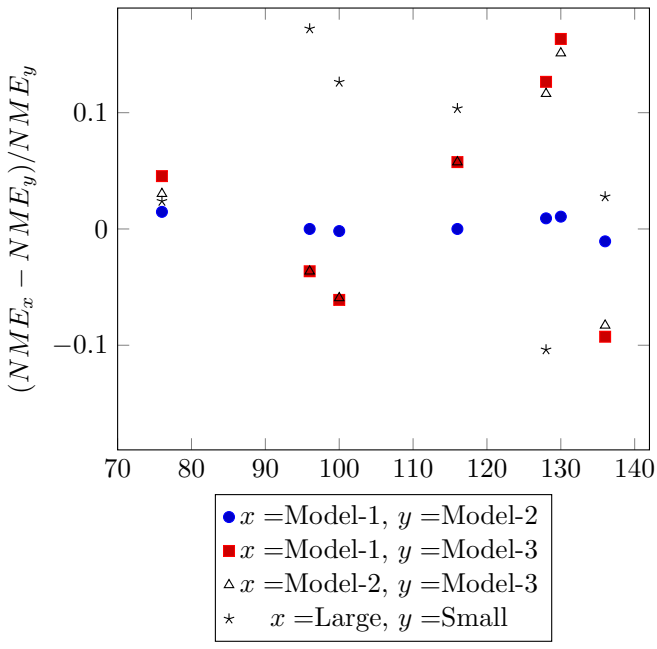

FIG. 8. Relative differences between the $0\nu\beta\beta$ NMEs calculated in the sp bases (except WS for $A = 116$) using different models for g_{ph} values. The asterisk describes differences between the NMEs of Ref. [29] and the combined results of Model 2 and Model 3, displayed in the second column of Table VI.

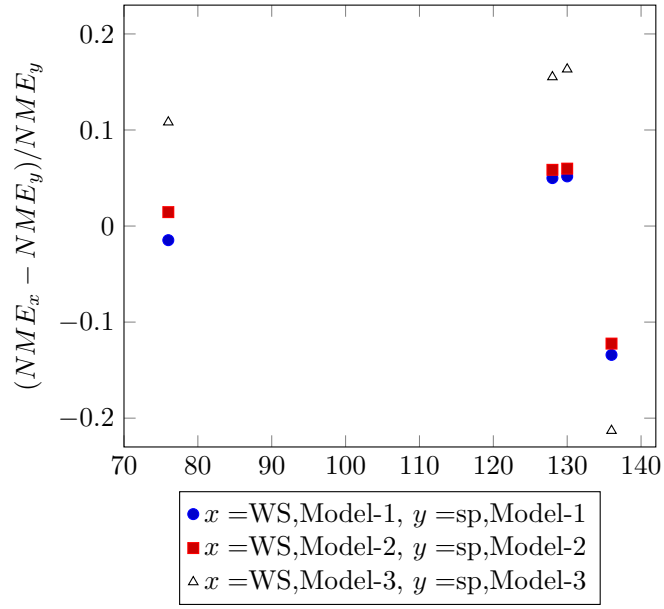

FIG. 9. Relative differences between the $0\nu\beta\beta$ NMEs calculated using different single-particle bases.

IV. CONCLUSIONS

In this work we calculated the nuclear matrix elements of the neutrinoless $\beta\beta$ decays mediated by the light Majorana neutrino. The matrix elements were computed for seven key decays of immediate experimental interest, and for which experimental data on isovector spin-dipole $J^\pi = 2^-$ giant resonances have become available. The calculations were performed using realistic two-body interactions and two different sets of no-core single-particle bases, the bare Woods-Saxon bases and their slightly modified versions, to better reproduce the experimental quasiparticle spectra of relevance to this study. In addition, we include up-to-date nucleon-nucleon short-range correlations, nucleon form factors, induced weak nucleonic currents, and partial restoration of isospin. We adjusted the g_{ph} parameter of the pnQRPA in two different ways: by fitting it to the location of the GT giant resonance (GTR) in the traditional way, and by fitting it to the location of the IVSD $J^\pi = 2^-$ giant resonance as a new method which has become possible because of new experimental data. We calculated the $0\nu\beta\beta$ NMEs using three methods: adopting the g_{ph} adjusted to GTR for each multipole, adjusting the $g_{\text{ph}}(2^-)$ separately to the IVSD $J^\pi = 2^-$ giant resonance, and adopting the $g_{\text{ph}}(2^-)$ for each multipole $J^\pi \neq 1^+$. Finally we compared the obtained results against each other and against a previous study of Hyvärinen *et al.* in which smaller single-particle model spaces were used.

The $0\nu\beta\beta$ NMEs computed in the present no-core modified-WS single-particle bases, using the IVSD $J^\pi = 2^-$ fitted g_{ph} values, deviate from the previously computed NMEs of Hyvärinen *et al.* [29], based on the g_{ph} adjusted by the empirical GT resonance energies, by less than 4% for the decays of ^{76}Ge and ^{136}Xe, and by some 10–18% for the rest of the cases. Most of the deviations are due to the extension of the single-particle space of pnQRPA, while the effect of adjusting

the particle-hole interaction to data on spin-dipole resonances is relatively smaller. Table VI summarizes our results for the nuclear-structure coefficients that reflect the improvements of the $0\nu\beta\beta$ NMEs achieved in the present work. The quoted errors only take into account the uncertainties due to the strength of the particle-hole interaction.

[1] J. Suhonen and O. Civitarese, Phys. Rep. **300**, 123 (1998).
[2] H. Ejiri, J. Phys. Soc. Jpn. **74**, 2101 (2005).
[3] J. D. Vergados, H. Ejiri, and F. Šimkovic, Rep. Prog. Phys. **75**, 106301 (2012).
[4] J. D. Vergados, H. Ejiri, and F. Šimkovic, Int. J. Mod. Phys. E **25**, 1630007 (2016).
[5] J. Engel and J. Menéndez, Rep. Prog. Phys. **80**, 046301 (2017).
[6] A. S. Barabash, Phys. Rev. C **81**, 035501 (2010).
[7] A. S. Barabash, Nucl. Phys. A **935**, 52 (2015).
[8] M. Agostini *et al.* (GERDA Collaboration), Nature (London) **544**, 47 (2017); Phys. Rev. Lett. **120**, 132503 (2018); R. Arnold *et al.* (NEMO-3 Collaboration), JETP Lett. **80**, 377 (2004); J. Argyriades *et al.* (NEMO-3 Collaboration), Nucl. Phys. A **847**, 168 (2010); R. Arnold *et al.* (NEMO-3 Collaboration), Phys. Rev. D **92**, 072011 (2015); **95**, 012007 (2017); K. Alfonso *et al.* (CUORE Collaboration), Phys. Rev. Lett. **115**, 102502 (2015); H. S. Antila and E. Luijten (CUORE Collaboration), *ibid.* **120**, 135501 (2018); J. B. Albert *et al.* (EXO-200 Collaboration), Nature (London) **510**, 229 (2014); Phys. Rev. Lett. **120**, 072701 (2018); A. Gando, Y. Gando, T. Hachiya, A. Hayashi, S. Hayashida, H. Ikeda, K. Inoue, K. Ishidoshiro, Y. Karino, M. Koga, S. Matsuda, T. Mitsui, K. Nakamura, S. Obara, T. Oura, H. Ozaki, I. Shimizu, Y. Shirahata, J. Shirai, A. Suzuki, T. Takai, K. Tamae, Y. Teraoka, K. Ueshima, H. Watanabe, A. Kozlov, Y. Takemoto, S. Yoshida, K. Fushimi, T. I. Banks, B. E. Berger, B. K. Fujikawa, T. ODonnell, L. A. Winslow, Y. Efremenko, H. J. Karwowski, D. M. Markoff, W. Tornow, J. A. Detwiler, S. Enomoto, M. P. Decowski (KamLAND-Zen Collaboration), *ibid.* **117**, 082503 (2016); C. E. Aalseth *et al.* (MAJORANA Collaboration), *ibid.* **120**, 132502 (2018).
[9] J. Suhonen and O. Civitarese, J. Phys. G **39**, 085105 (2012).
[10] J. Toivanen and J. Suhonen, Phys. Rev. Lett. **75**, 410 (1995).
[11] C. M. Raduta and A. A. Raduta, Phys. Rev. C **82**, 068501 (2010).
[12] E. Caurier, J. Menéndez, F. Nowacki, and A. Poves, Phys. Rev. Lett. **100**, 052503 (2008).
[13] J. Menéndez, A. Poves, E. Caurier, and F. Nowacki, Nucl. Phys. A **818**, 139 (2009).
[14] J. Barea and F. Iachello, Phys. Rev. C **79**, 044301 (2009).
[15] T. R. Rodríguez and G. Martínez-Pinedo, Phys. Rev. Lett. **105**, 252503 (2010).
[16] N. L. Vaquero, T. R. Rodriguez, and J. L. Egido, Phys. Rev. Lett. **111**, 142501 (2013).
[17] P. K. Rath, R. Chandra, K. Chaturvedi, P. K. Raina, and J. G. Hirsch, Phys. Rev. C **82**, 064310 (2010).
[18] J. M. Yao, L. S. Song, K. Hagino, P. Ring, and J. Meng, Phys. Rev. C **91**, 024316 (2015).
[19] L. S. Song, J. M. Yao, P. Ring, and J. Meng, Phys. Rev. C **95**, 024305 (2017).
[20] M. Horoi and B. A. Brown, Phys. Rev. Lett. **110**, 222502 (2013).
[21] R. A. Sen'kov and M. Horoi, Phys. Rev. C **90**, 051301(R) (2014).
[22] B. A. Brown, D. L. Fang, and M. Horoi, Phys. Rev. C **92**, 041301(R) (2015).
[23] Y. Iwata, N. Shimizu, T. Otsuka, Y. Utsuno, J. Menéndez, M. Honma, and T. Abe, Phys. Rev. Lett. **116**, 112502 (2016).
[24] J. Suhonen and O. Civitarese, J. Phys. G **39**, 124005 (2012).
[25] J. Suhonen and O. Civitarese, Nucl. Phys. A **847**, 207 (2010).
[26] J. Suhonen, Nucl. Phys. A **853**, 36 (2011).
[27] O. Civitarese, H. Müther, L. D. Skouras, and A. Faessler, J. Phys. G **17**, 1363 (1991).
[28] F. Šimkovic, V. Rodin, A. Faessler, and P. Vogel, Phys. Rev. C **87**, 045501 (2013).
[29] J. Hyvärinen and J. Suhonen, Phys. Rev. C **91**, 024613 (2015).
[30] J. Barea, J. Kotila, and F. Iachello, Phys. Rev. C **91**, 034304 (2015).
[31] J. Suhonen, *From Nucleons to Nucleus: Concepts of Microscopic Nuclear Theory* (Springer, Berlin, 2007).
[32] M. Kortelainen, O. Civitarese, J. Suhonen, and J. Toivanen, Phys. Lett. B **647**, 128 (2007).
[33] M. Kortelainen and J. Suhonen, Phys. Rev. C **75**, 051303(R) (2007).
[34] M. Kortelainen and J. Suhonen, Phys. Rev. C **76**, 024315 (2007).
[35] L. Jokiniemi and J. Suhonen, Phys. Rev. C **96**, 034308 (2017).
[36] A. Bohr and B. R. Mottelson, *Nuclear Structure, Vol. I* (Benjamin, New York, 1969).
[37] K. Holinde, Phys. Rep. **68**, 121 (1981).
[38] J. Suhonen, T. Taigel, and A. Faessler, Nucl. Phys. A **486**, 91 (1988).
[39] J. Suhonen, Nucl. Phys. A **563**, 205 (1993).
[40] J. Suhonen, Nucl. Phys. A **700**, 649 (2002).
[41] NuDat 2.6, Brookhaven National Laboratory, National Nuclear Data Center, http://www.nndc.bnl.gov/nudat2/.
[42] J. Kotila and F. Iachello, Phys. Rev. C **85**, 034316 (2012).
[43] D.-L. Fang, A. Faessler, V. Rodin, and F. Šimkovic, Phys. Rev. C **82**, 051301 (2010).
[44] J. Terasaki, Phys. Rev. C **91**, 034318 (2015).
[45] G. A. Miller and J. E. Spencer, Ann. Phys. (NY) **100**, 562 (1976).
[46] F. Šimkovic, A. Faessler, H. Müther, V. Rodin, and M. Stauf, Phys. Rev. C **79**, 055501 (2009).
[47] D.-L. Fang, A. Faessler, and F. Šimkovic, Phys. Rev. C **97**, 045503 (2017).
[48] P. Vogel and M. R. Zirnbauer, Phys. Rev. Lett. **57**, 3148 (1986).
[49] O. Civitarese, A. Faessler, and T. Tomoda, Phys. Lett. B **194**, 11 (1987).
[50] C. Gaarde, J. S. Larsen, M. N. Harakeh, S. Y. van der Werf, M. Igarashi, and A. Müller-Arnke, Nucl. Phys. A **334**, 248 (1980).
[51] C. D. Goodman, Nucl. Phys. A **374**, 241c (1982).
[52] H. Akimune, I. Daito, Y. Fujita, M. Fujiwara, M. B. Greenfield, M. N. Harakeh, T. Inomata, J. Jänecke, K. Katori, S. Nakayama *et al.*, Phys. Rev. C **52**, 604 (1995).
[53] J. H. Thies, D. Frekers, T. Adachi, M. Dozono, H. Ejiri, H. Fujita, M. Fujiwara, E.-W. Grewe, K. Hatanaka, P. Heinrichs *et al.*, Phys. Rev. C **86**, 014304 (2012).
[54] J. H. Thies, P. Puppe, T. Adachi, M. Dozono, H. Ejiri, D. Frekers, H. Fujita, Y. Fujita, M. Fujiwara, E.-W. Grewe *et al.*, Phys. Rev. C **86**, 054323 (2012).
[55] J. H. Thies, T. Adachi, M. Dozono, H. Ejiri, D. Frekers, H. Fujita, Y. Fujita, M. Fujiwara, E.-W. Grewe, K. Hatanaka *et al.*, Phys. Rev. C **86**, 044309 (2012).

[56] H. Akimune, H. Ejiri, M. Fujiwara, I. Daito, T. Inomata, R. Hazama, A. Tamii, H. Toyokawa, and M. Yosoi, Phys. Lett. B **394**, 23 (1997).
[57] P. Puppe, A. Lennarz, T. Adachi, H. Akimune, H. Ejiri, D. Frekers, H. Fujita, M. Fujiwara, E. Ganioğlu, E.-W. Grewe *et al.*, Phys. Rev. C **86**, 044603 (2012).
[58] P. Puppe, D. Frekers, T. Adachi, H. Akimune, N. Aoi, B. Bilgier, H. Ejiri, H. Fujita, Y. Fujita, M. Fujiwara *et al.*, Phys. Rev. C **84**, 051305 (2011).
[59] H. Ejiri, K. Ikeda, and J. I. Fujita, Phys. Rev. **176**, 1277 (1968).
[60] F. Šimkovic, A. Faessler, V. A. Rodin, P. Vogel, and J. Engel, Phys. Rev. C **77**, 045503 (2008).
[61] J. Suhonen and M. Kortelainen, Int. J. Mod. Phys. E **17**, 1 (2008).
[62] M. Aunola and J. Suhonen, Nucl. Phys. A **602**, 133 (1996).
[63] J. Suhonen, Phys. Lett. B **607**, 87 (2005).
[64] J. Suhonen and O. Civitarese, Phys. Lett. B **725**, 153 (2013).
[65] J. Suhonen and O. Civitarese, Nucl. Phys. A **924**, 1 (2014).
[66] Z. M. Niu, Y. F. Niu, H. Z. Liang, W. H. Long, and J. Meng, Phys. Rev. C **95**, 044301 (2017).